ELSEVIER

Journal of Magnetism and Magnetic Materials 192 (1999) 238–246

Journal of magnetism and magnetic materials

Hydrogen induced changes of the interlayer coupling in $Fe_{(3)}/V_{(x)}$ superlattices ($x = 11$–16)

D. Labergerie[a], C. Sutter[a], H. Zabel[a,*], B. Hjörvarsson[b]

[a]*Ruhr-Universität Bochum, Lehrstuhl für Experimentalphysik/Festkörperphysik, D-44780 Bochum, Germany*
[b]*Royal Institute of Technology, Materialphysics, S-100 44 Stockholm, Sweden*

Received 24 July 1998; received in revised form 8 October 1998

Abstract

The effect of hydrogen on the magnetic exchange coupling between iron layers through vanadium spacer layers has been studied with magneto-optical Kerr effect experiments in $Fe_{(3)}/V_{(x)}$ superlattices. Here x refers to the number of V monolayers varying from 11 to 16 and the Fe layer thickness is fixed at three monolayers. Without hydrogen the superlattice is antiferromagnetic (AFM) for x between 12 and 14 and ferromagnetic (FM) in all other cases. With hydrogen loading the coupling can be switched from AFM to FM and vice versa. As previously observed with neutron reflectivity measurements (Hjörvarsson et al., Phys. Rev. Lett. 79 (1997) 901) the change of the interlayer coupling upon hydrogen uptake is not simply due to the expansion of the non-magnetic vanadium spacer layer but more likely to the distortion of the Fermi surface. Bilinear and biquadratic exchange couplings can be recognized by the magnetic hysteresis loops and their coupling energies have been extracted by fits to the curves. For all samples the easy axis of the magnetization is in the plane without any preferred in-plane direction. Hydrogen loading does not affect the magnetic anisotropy of these samples.

Keywords: Interlayer exchange coupling; Anisotropy; Superlattice; MOKE

1. Introduction

Since the first discovery of the exchange coupling of Fe layers through Cr spacer layers by Grünberg et al. in 1986 [1], much experimental and theoretical work has been devoted to this broad and promising field. It has been shown that the magnetic coupling in Fe/Cr multilayers oscillates with increasing Cr spacer layer thickness between ferromagnetic and antiferromagnetic, exhibiting a short oscillation period of about 2 monolayers (ML) [2,19,20] superposed on a longer period of about 22 ML [3]. Concomitantly, a giant magnetoresistance effect with a period commensurate with the exchange coupling period was discerned soon after [4,21]. Fe/Cr heterostructures and superlattices were the first system which has been extensively studied and for which most of the important properties of exchange coupled superlattices have been unraveled. At the same time, the fast development of deposition techniques via

* Corresponding author. Tel.: + 49-234-700-36-49; fax: + 49-234-709-41-73; e-mail: hartmut.zabel@ruhr-uni-bochum.de.

0304-8853/99/$ – see front matter
PII: S0304-8853(98)00546-0

sputtering and MBE methods allowed fabricating high quality ultrathin films, trilayers, multilayers, and superlattices of a number of other systems that has triggered much experimental effort to investigate their intriguing magnetic and transport properties (For a most recent update of the development in the field see for example, Refs. [5,22]). Most recently, very exciting polarized neutron reflectivity experiments have been performed on sputtered $Fe_{(3)}/V_{(x)}$ superlattices investigating spin structures and exchange couplings and how these properties are altered by hydrogen uptake in the vanadium spacer layers [6]. Here the subscripts indicate the number of Fe and V monolayers period. In particular, upon loading the multilayer with hydrogen a switching from antiferromagnetic (AFM) to ferromagnetic (FM) exchange coupling and vice versa was observed. This is similar to the changes of the exchange coupling which have previously been observed upon hydrogen loading of Fe/Nb multilayers [7]. In general, hydrogen loading causes a volume expansion of the host lattice which is linearly proportional to the hydrogen concentration [8]. In case of epitaxial films with elastic boundary conditions prohibiting an in-plane expansion, the out-of-plane expansion (parallel to the film normal) can reach up to 10%, as observed for $Fe_{(3)}/V_{(x)}$ superlattices [9,10]. Hjörvarsson et al. could, however, show that the vanadium lattice expansion is not the major cause for the switching behavior of the interlayer exchange coupling [6]. The superlattice containing 15 ML of V is at the border line between AFM and FM coupling. Instead of becoming FM coupled upon hydrogen loading, as one would expect from an expanding V layer thickness, this superlattice becomes AFM coupled for a limited hydrogen concentration range indicative for a specific distortion of the vanadium Fermi surface, thereby creating new spanning vectors for the exchange coupling.

The neutron reflectivity experiments could prove the existence of coherent AFM and FM spin structures in the Fe/V superlattices and determine qualitatively the coupling strengths. However, for a more quantitative analysis it is necessary to determine complete magnetic hysteresis loops. They allow us to extract more detailed information about the type of coupling (bilinear, biquadratic) and to determine the coupling energies between the iron layers through the vanadium spacers as a function of the spacer thickness and the hydrogen concentration.

In the following, we present extensive longitudinal magneto-optical Kerr measurements of the magnetic hysteresis of $Fe_{(3)}/V_{(x)}$ ($x = 11$–16) superlattices with and without hydrogen.

These are the first hysteresis measurements on Fe/V(0 0 1) superlattices with Fe layer thickness of only 3 ML. Extensive magnetic measurements on Fe/V multilayers and superlattices containing thicker Fe layers have been reported previously by Granberg et al. [11].

2. Experimental details

A series of Fe/V superlattices all composed of three monolayers of iron and with varying vanadium thicknesses (from 11 to 16 MLs) has been investigated via the magneto-optical Kerr effect in the longitudinal configuration. The samples were sputter grown on epi-polished MgO [1 0 0] substrates, as described in more detail in Ref. [12]. They were all covered with a 3 nm Pd cap layer to allow a fast uptake and release of hydrogen at a temperature of less than 100°C and to avoid oxidation of the sample. The total number of double layers in this set of samples is $N = 30$. Prior to hydrogen exposure, the samples were characterized with small angle X-ray reflectivity measurements using Mo–Kα_1 radiation ($\lambda = 0.0709$ nm). A representative reflectivity curve of the $Fe_{(3)}/V_{(13)}$ sample is shown in Fig. 1. The solid line is a fit to the data points using a generalized Parratt algorithm [13,23]. The first and second order superlattice reflections as well as the finite size oscillations are well pronounced, proving the high structural quality of the superlattice with a low interface roughness of typically less than 1 ML. The nominal (Λ_{nom}), as provided by the growth parameters, and the actually measured (Λ_{meas}) bilayer periods of the samples investigated here are listed in Table 1.

The magnetic hysteresis of the $Fe_{(3)}/V_{(x)}$ superlattices have been investigated with an improved magneto-optical Kerr effect (MOKE) setup developed in one of our laboratory facilities [14,24].

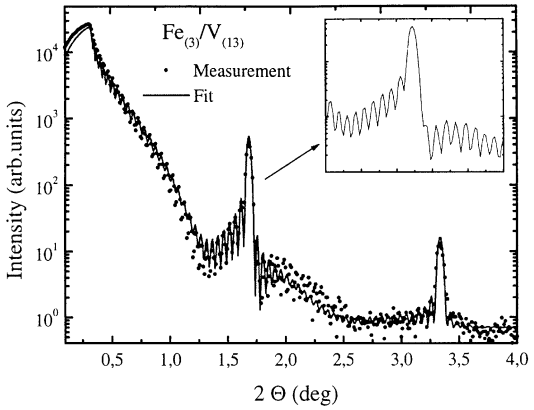

Fig. 1. Small angle X-ray reflectivity of the $Fe_{(3)}/V_{(13)}$ superlattice before loading with hydrogen. The solid line is a fit to the data points using a generalized Parratt algorithm.

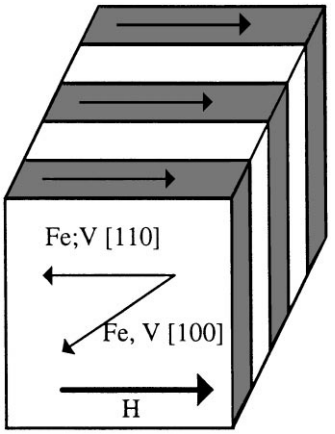

Fig. 2. Schematics of the sample orientation and the scattering geometry for longitudinal MOKE measurements. The MOKE measurements were performed with a magnetic field along the [1 1 0] axis, which is the hard axis in bulk samples. In our geometry the [1 0 0] axis is oriented along the film diagonal.

We briefly outline the basic features of this technique and the refinement used to increase the sensitivity of the measurements. MOKE is based on the change of the polarization state of incident light reflected by magnetic materials [15]. In the longitudinal configuration, this change is directly proportional to the in-plane magnetization of the material [16]. In our case, the plane of polarization of the He–Ne laser beam ($\lambda = 632.8$ nm, $P = 5$ mW) was aligned perpendicular to the plane of incidence (s-state). A Faraday modulation lock-in technique has been implemented in the standard setup to obtain a better resolution of the detected signal. The linear polarization state of the laser beam reflected by the sample is modulated sinoidally by passing through a Faraday rod. A second Faraday rod, installed downstream, turns the polarization state in such way that the signal measured is minimized. For more details see Refs. [14,24]. This refinement in the detection allows us to commonly reach an angular resolution of better than 2×10^{-4} deg, which corresponds in the case of Fe layers to a magnetization of 40 emu/cm^3.

The MOKE measurements were performed at room temperature along the [1 1 0] axis, which is the projection of the hard axis of the bulk iron in the film plane (see Fig. 2). The penetration depth (~ 50 nm) allows us to see a large number (~ 20) of double layers without being disturbed by the substrate. The sample was positioned in a high vacuum chamber in the center of a magnetic field. Due to the required pole distance the maximum field was limited to 2000 Oe. The vacuum chamber was connected to a hydrogen loading facility allowing an exposure of the sample up to a hydrogen gas pressure of 900 mbar. This pressure is more than sufficient to saturate the sample with hydrogen [9,10].

Table 1
Structural parameters of the different samples investigated

Sample	$Fe_{(3)}/V_{(11)}$	$Fe_{(3)}/V_{(12)}$	$Fe_{(3)}/V_{(13)}$	$Fe_{(3)}/V_{(14)}$	$Fe_{(3)}/V_{(15)}$	$Fe_{(3)}/V_{(16)}$
N	30	30	30	30	30	30
Λ_{nom} (Å)	20.9	22.4	23.9	25.5	27	28.5
Λ_{meas} (Å)	20.9	21.9	24.4	25.8	27.3	27.5
Rel. deviation (%)	0	− 2.2	2.1	1.2	1.1	3.5

The pressure was measured via a strain gauge with a relative accuracy of 0.5%. The most important changes of the exchange coupling take place at rather low hydrogen pressures between 0 and 15 mbar. In this pressure range the measurements are completely reversible and zero hydrogen pressure corresponds to an essentially hydrogen free sample, while at 10 mbar the estimated hydrogen concentration in the vanadium layers is about 20%. Since the signal detected is only 10 times the resolution limit of our system, we have taken several measurements (typically 5) at any given point and averaged them to improve the signal to noise ratio. Using a thin paramagnetic Nb film we have detected a non-negligible Faraday rotation due to the optical windows of our hydrogen loading facility, which subsequently was subtracted from all our measurements. The time between each pressure step was at least 20–30 min in order to reach an equilibrium state of the sample and to guarantee a homogeneous hydrogen distribution in the sample.

3. Results and discussions

3.1. MOKE measurements

In Fig. 3 the longitudinal MOKE hysteresis loops measured in the experimental configuration as depicted in Fig. 2 are presented. All measurements were performed at room temperature on $Fe_{(3)}/V_{(x)}$ superlattices with x varying from 11 to 16 ML and for different hydrogen pressures. Each column of Fig. 3 corresponds to one particular superlattice as indicated, and each row corresponds to different representative hydrogen pressures, starting at zero pressures in the first row, a medium hydrogen pressure ($\sim$5 mbar) in the middle row, and finally a high pressures ($\sim$10 mbar) in the bottom row. For the unloaded samples one can easily recognize that the magnetic coupling oscillates between FM and AFM as a function of the vanadium thickness. The period of this oscillation is on the order of 3 MLs ($Fe_{(3)}/V_{(12)}$ and $Fe_{(3)}/V_{(14)}$ are AFM). The hysteresis curve for an antiferromagnetically coupled system is characterized by a linear slope as a function of the applied field

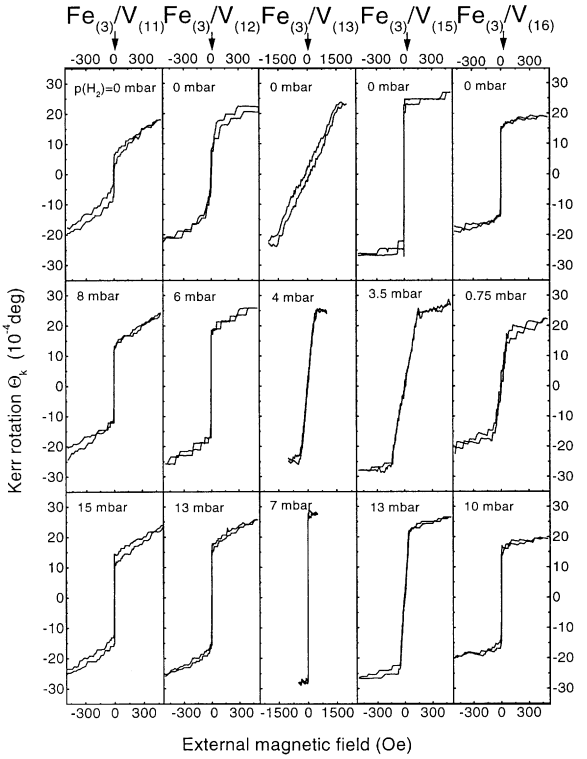

Fig. 3. Longitudinal MOKE hysteresis loops of $Fe_{(3)}/V_{(x)}$ superlattices with x varying from 11 to 16 and at different hydrogen pressures measured at room temperature. The columns show data for a particular sample, the rows data are for zero hydrogen pressure (1st row), intermediate hydrogen pressures (2nd row), and high hydrogen pressures (3rd row). The switching of the magnetic coupling from FM (characterized by a square shape with a remanent magnetization) to AFM (hysteresis curve with a linear slope at small field values and negligible remanent magnetization) and vice versa with changing V thickness and hydrogen pressure can already be seen by inspection of the raw data (see also text).

and a very small remanent magnetization (e.g. $Fe_{(3)}/V_{(13)}$ without hydrogen), whereas for a ferromagnetically coupled system the hysteresis exhibits more a square like shape with a rather large remanent magnetization (e.g. $Fe_{(3)}/V_{(15)}$ without hydrogen). The $Fe_{(3)}/V_{(11,12)}$ samples exhibit, in addition to the ferro or antiferromagnetic shape, also biquadratic (90°) coupling contributions [17], discernible by the slow saturation of the magnetization with increasing external field. It is interesting to note that for the FM coupled systems the Kerr

angle in remanence to respect to the Kerr angle saturation increases with the number of vanadium MLs. This may be due to an improving structural quality of the superlattices with increasing vanadium thickness.

Next we study the development of the hysteresis loops along the columns. For the first two superlattices ($Fe_{(3)}/V_{(11,12)}$) we notice that the remanent Kerr rotation increases with increasing hydrogen pressure. Furthermore, these samples exhibit at the highest hydrogen pressure saturation fields which were outside the measurement range. It appears that hydrogen induces a stronger biquadratic coupling in these samples. While the overall shape of the hysteresis loops does not change for these first two superlattices, we recognize dramatic changes for all other superlattices with increasing hydrogen pressure (concentration). The superlattice $Fe_{(3)}/V_{(13)}$ changes shape from AFM to FM, superlattice $Fe_{(3)}/V_{(15)}$ from FM to AFM, and finally the superlattice $Fe_{(3)}/V_{(16)}$ starts FM like, changes to AFM at low pressures and returns to FM at higher pressures.

In Fig. 4, the remanent Kerr rotation and the saturation field extracted from the measurements are plotted as function of the hydrogen pressure. Different interesting features in this figure are worth noting. First, hydrogen loading of the $Fe_{(3)}/V_{(15)}$ superlattice leads to a resonance like AFM coupling between 1 and 8 mbar. Indeed, if we consider the oscillatory exchange coupling of $Fe_{(3)}/V_{(x)}$ as a function of the number of MLs x, for $x = 15$–16 we expect FM coupling, and for $x > 16$ again AFM coupling. In contrast, only a slight hydrogen pressure (~ 1 mbar) in the $Fe_{(3)}/V_{(15)}$ superlattice causing only a small lattice expansion causes, however, a dramatic change of the coupling nature. This clearly proves that the lattice expansion cannot explain the change of the coupling nature as already noted previously [6]. At higher hydrogen pressures the coupling on the $Fe_{(3)}/V_{(15)}$ does not completely return to the FM type but shows a residual AFM contribution, with a saturation field on the order of 40 Oe. This result could not be observed by the neutron reflectivity measurements [6] because of the constant external neutron guide field which was set to 100 Oe. At this field level the superlattice appears already FM coupled (see Fig. 3). In the $Fe_{(3)}/V_{(13)}$ sample, FM coupling occurs at a hydrogen pressure where the sample should still be AFM coupled as concerns the vanadium layer thickness. In Table 2 we summarize the magnetic couplings and the saturation fields for the $Fe_{(3)}/V_{(x)}$ superlattices as determined by MOKE measurements for the unloaded and loaded samples with hydrogen.

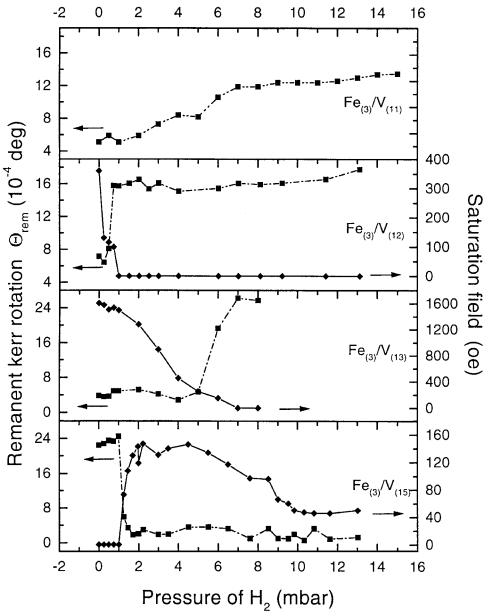

Fig. 4. Remanent Kerr rotation and saturation field as a function of the hydrogen pressure for different samples extracted from the longitudinal MOKE hysteresis loops at room temperature.

It has been observed previously with FMR measurements that in Fe/V superlattices with only 3 MLs of Fe the easy axis is in the plane and that there is no in-plane anisotropy [18]. We have characterized the magnetic anisotropy of the $Fe_{(3)}/V_{(13)}$ superlattice before and after hydrogen loading of the sample in order to test whether these properties depend on the hydrogen concentration. Fig. 5 reproduces hysteresis loop of the sample exposed to 800 mbar hydrogen pressure and with the external field applied along the [1 1 0] axis (line) and the [1 0 0] axis (diamonds). The difference between these two hysteresis loops is shown by filled squares. Within the resolution of our system the

Table 2
Summary of the exchange coupling as deduced from magneto-optical Kerr effect measurements

Sample	$Fe_{(3)}/V_{(11)}$	$Fe_{(3)}/V_{(12)}$	$Fe_{(3)}/V_{(13)}$	$Fe_{(3)}/V_{(14)}$	$Fe_{(3)}/V_{(15)}$	$Fe_{(3)}/V_{(16)}$
Coupling without H_2	FM	AFM	AFM	AFM	FM	FM
H_{sat} (Oe)		360	1600	700		
Coupling with H_2	FM	Becomes FM	Becomes FM	No result	AFM Resonance	AFM Resonance
H_{sat} (Oe)					150	115

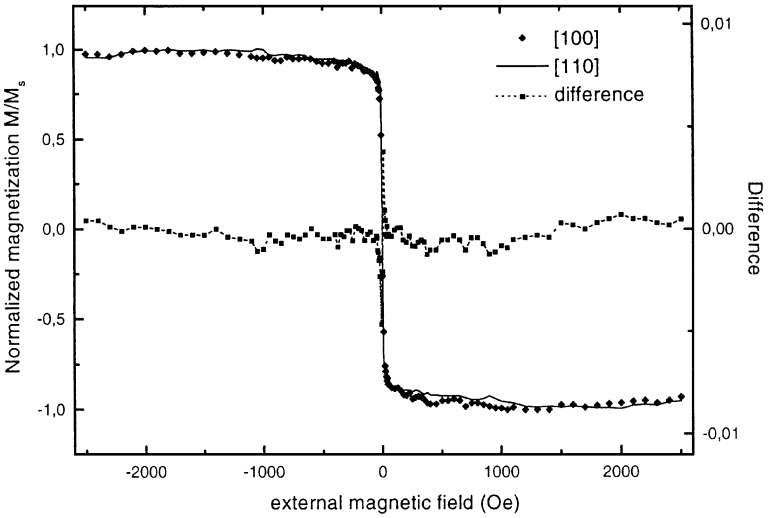

Fig. 5. Comparison between the hysteresis loops with external magnetic fields applied along the [1 1 0] and the [1 0 0] axis on the $Fe_{(3)}/V_{(13)}$ superlattice and at a constant hydrogen pressure of 800 mbar at room temperature.

sample remains isotropic even at these high hydrogen pressures. This is a surprising result, since the hydrogen uptake causes a large change of the vanadium sublattices and eventually one on the crystal fields at the Fe/V interface. Therefore, an effect of hydrogen on the magnetic anisotropy would have been conceivable.

3.2. Analysis and computer simulation

We analyzed the magnetic hysteresis loops using a simple phenomenological model containing no in-plane anisotropy as justified by the present MOKE results (Fig. 5) and by earlier FMR measurements [18]. The magnetic energy per unit area of a superlattice with N double layers can then be written as [17]

$$E = -\sum_{i=1}^{N} M_S t_{Fe} H \cos(\Phi_i - \Theta_H) - \sum_{i=1}^{N-1} J_{BL} \cos(\Phi_i - \Phi_{i+1}) - \sum_{i=1}^{N-1} J_{BQ} \cos^2(\Phi_i - \Phi_{i+1}). \quad (1)$$

Here the first term in Eq. (1) corresponds to the Zeeman energy, the second to the bilinear exchange coupling characterized by a bilinear coupling constant J_{BL} between two adjacent Fe layers, and the third to the biquadratic coupling J_{BQ}. Φ_i is the angle between the [1 0 0] direction and the

magnetic moment in the layer i, and Θ_H the angle between the [1 0 0] direction and the applied field H. M_s is the magnetization in saturation and t_{Fe} is the Fe layer thickness. The fit program searches the energies J_{BL} and J_{BQ} that minimizes the total energy E with respect to the angle Φ_i. The procedure is then repeated for each field value H. If we assume that the magnetization vectors in two adjacent Fe layers are antiparallel (pure antiferromagnetic coupling: $\Phi_i = -\Phi_{1+1}$, and $J_{BQ} = 0$), it is possible to directly evaluate the coupling constant J_{AF}, from the saturation field H_s according to

$$J_{AF} = \frac{N}{4(N-1)} H_S M_S t_{Fe}. \quad (2)$$

The saturation magnetization values, M_s, of our samples used to fit the hysteresis loops were determined independently by FMR measurements at room temperature and at a frequency of 9.2 GHz. The magnetic field of 13 kOe sufficient for saturating the samples was applied along the [1 1 0] in-plane direction. The results are listed in Table 3. The relatively small magnetization values of the $Fe_{(3)}/V_{(13)}$ superlattice is probably due to a smaller thickness of the Fe layer compared to the samples used in Ref. [18] or to a smaller magnetic moment of the Fe atoms at the interface between iron and vanadium. Using the linear dependence of the saturation magnetization (per iron volume) for Fe/V multilayers to the inverse of the number of periods n, Poulopoulos et al. have found that the Fe magnetic moment at the interface should be reduced by a factor of 0.32 as compared to bulk iron [18]. In other words, Fe monolayers embedded between nearest neighbor Fe MLs exhibit the bulk magnetic moment of 2.2 μ_B, whereas Fe monolayers at the interface to vanadium show a reduced moment of $0.32 \times 2.2\ \mu_B = 0.7\ \mu_B$. Our magnetization measurements indicate that not only the boundary Fe layers exhibit a reduced moment but also the interior Fe layer.

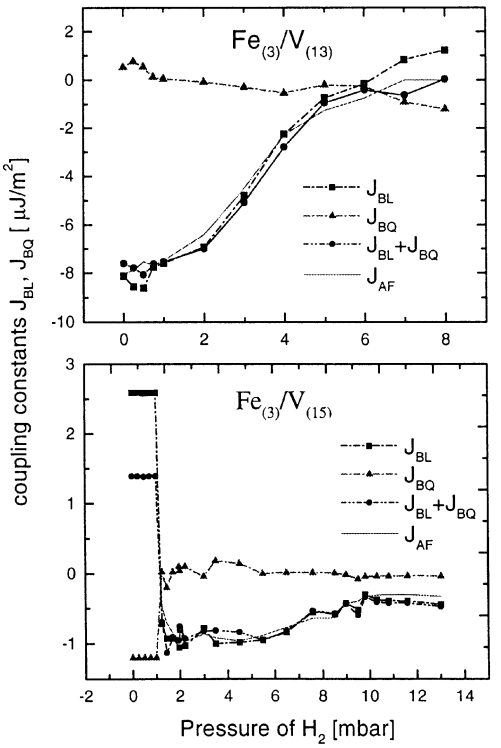

Fig. 6. Bilinear and biquadratic coupling energies extracted from the fit of the hysteresis loops for two superlattices which switch their exchange coupling nature with increasing hydrogen pressure. Top panel: $Fe_{(3)}/V_{(13)}$, bottom panel: $Fe_{(3)}/V_{(15)}$.

Returning to the coupling nature of the superlattices, we have plotted in Fig. 6 the variation of the bilinear (J_{BL}) and biquadratic (J_{BQ}) coupling energies as well as their sum ($J_{BL} + J_{BQ}$) versus the hydrogen pressure for two respective samples (see also Table 4). We also show the AFM coupling constant (J_{AF}) as calculated directly via Eq. (2). We should note that for strongly AFM coupled

Table 3
Saturation magnetization of the Fe layers in the Fe/V superlattices as determined by ferromagnetic resonance (FMR) at room temperature

Sample	$Fe_{(3)}/V_{(11)}$	$Fe_{(3)}/V_{(12)}$	$Fe_{(3)}/V_{(13)}$	$Fe_{(3)}/V_{(15)}$	Bulk
$4\pi M_s$ (emu/cm^3)	469	536	417	549	1740

Table 4
Bilinear and biquadratic coupling energies determined for Fe/V superlattices with and without hydrogen

	Sample	$Fe_{(3)}/V_{(11)}$	$Fe_{(3)}/V_{(12)}$	$Fe_{(3)}/V_{(13)}$	$Fe_{(3)}/V_{(14)}$	$Fe_{(3)}/V_{(15)}$	$Fe_{(3)}/V_{(16)}$
$p(H_2) = 0$	J_{BL}	− 3.6	− 2.0	− 8.1	− 4.1	+ 2.6	− 1.8
	J_{BQ}	− 1.8	− 1.3	+ 0.5	+ 0.2	− 1.2	− 2.0
	$\mu J/m^2$						
$p(H_2) \neq 0$				8 mbar		4 mbar	
	J_{BL}			+ 1.2	no result	− 1.0	
	J_{BQ}			− 1.2		+ 0.1	
	$\mu J/m^2$						

superlattices the biquadratic coupling is very small as compared to the bilinear one and can be neglected. The biquadratic coupling is more important for superlattices at the border line between FM and AFM coupled systems and appears to increase with hydrogen pressure as mentioned before. In this respect the biquadratic coupling contribution can be considered as a precursor to AFM coupling. In a purely FM and AFM coupled superlattice, the lateral fluctuation between both exchange couplings can be neglected. However, in superlattices which are fine-tuned by the hydrogen content to the border between FM and AFM coupling, minute lateral thickness fluctuations become noticeable and contribute to the biquadratic coupling. This aspect will be worked out in the future in more detail.

4. Summary

In summary, we have performed magneto-optical Kerr measurements on $Fe_{(3)}/V_{(x)}$ superlattices with x varying from 11 to 16 in order to determine quantitatively the exchange coupling constant between two adjacent iron layers separated by different thicknesses of vanadium spacer layers. A small and continuous variation of the vanadium thickness has been achieved by loading the sample with hydrogen. But more important are the changes of the electronic structure induced by the hydrogen loading. We find that with hydrogen the coupling can continuously be changed from AFM to FM and from FM to AFM. In some cases the coupling starts from FM, switches to AFM with increasing hydrogen concentration and returns to FM at the highest hydrogen concentration. We found that most hysteresis loops can successfully be simulated with a model that takes bilinear and biquadratic exchange coupling terms into account. In FM coupled superlattices the biquadratic coupling constant appears to increase with hydrogen concentration, whereas in AFM coupled superlattices the biquadratic contribution can be neglected. The experiments clearly show that hydrogen has a dramatic effect on the coupling nature of Fe/V superlattices, which cannot be explained solely on the basis of the lattice expansion as a function of the hydrogen concentration. Changes of the vanadium Fermi surface upon hydrogen loading creating new spanning vectors for the exchange coupling are required to explain these observations. In contrast, hydrogen has no effect on the magnetic anisotropy of the Fe layers. The magnetization vector of the Fe layers remains in-plane and exhibits no magnetocrystalline anisotropy at room temperature without and with hydrogen.

Acknowledgements

We would like to thank Jens Pflaum for his help with the FMR measurements, and Till Schmitte for his assistance during the MOKE measurements, and P. Isberg for growing the samples. This work was supported by the Bundesministerium für Bildung, Wissenschaft, Forschung und Technologie under contract 03-ZA4BC1-0, by the EU-TMR

network FMRX-CT98-0187. H.Z. would like to thank the Volkswagen-Stiftung for support during his sabbatical and BH acknowledges financial support from NFR.

References

[1] P. Grünberg, R. Schreiber, Y. Pang, M.B. Brodsky, C.H. Sowers, Phys. Rev. Lett. 57 (1986) 2442.
[2] J. Unguris, R.J. Celotta, D.T. Pierce, Phys. Rev. Lett. 67 (1991) 140.
[3] S.S.P. Parkin, N. More, K.P. Roche, Phys. Rev. Lett. 64 (1990) 2304.
[4] M.N. Baibich, J.M. Broto, A. Fert, F. Nguyen, Van Dau, F. Petroff, P. Etienne, G. Creuset, A. Friederich, J. Chazelas, Phys. Rev. Lett. 61 (1988) 2472.
[5] J. Tobin et al., Magnetic Ultrathin Films, Multilayers and Surfaces, MRS Symp. Proc., vol. 475, 1997.
[6] B. Hjörvarsson, J.A. Dura, P. Isberg, T. Watanabe, T.J. Udovic, G. Andersson, G.F. Majkrzak, Phys. Rev. Lett. 79 (1997) 901.
[7] F. Klose, Ch. Rehm, D. Nagengast, H. Maletta, A. Weidinger, Phys. Rev. Lett. 78 (1997) 1150.
[8] J. Peisl, in: G. Alefeld, J. Völkl (Eds.), Hydrogen in Metals I. Topics in Applied Physics, vol. 28, Springer, Berlin, 1978.
[9] G. Andersson, B. Hjörvasson, P. Isberg, Phys. Rev. B 55 (1997) 1774.
[10] G. Anderson, B. Hjörvarsson, H. Zabel, Phys. Rev. B 55 (1997) 15905.
[11] P. Granberg, P. Nordblad, P. Isberg, B. Hjörvarsson, R. Wäppling, Phys. Rev. B. 54 (1996) 1199.
[12] P. Isberg, B. Hjörvarsson, R. Wäppling, E.B. Svedberg, L. Hultman, Vacuum 48 (1997) 483.
[13] A. Abromeit, Diploma Thesis, Ruhr-Universität Bochum, 1992.
[14] T. Zeidler, Ph. D. Thesis, Ruhr-Universität Bochum, 1997.
[15] M. Born, E. Wolf, Principle of Optics, Pergamon Press, Oxford, 1989.
[16] S.D. Bader, J. Magn. Magn. Mater. 100 (1991) 440.
[17] M. Rührig, R. Schäfer, A. Hubert, R. Mosler, J.A. Wolf, J. Appl. Phys. 69 (1991) 4780.
[18] P. Poulopolous, P. Isberg, W. Platow, W. Wisny, M. Farle, B. Hjörvarsson, J. Magn. Magn. Mater. 170 (1997) 57.
[19] S.T. Purcell, W. Folkerts, M.T. Johnson, N.W.E. McGee, K. Jager, J. aan de Stegge, W.B. Zeper, W. Hoving, P. Gründberg, Phys. Rev. Lett. 67 (1991) 903.
[20] S. Demokritov, J.A. Wolf, P. Gründberg, Europhysics Letters 15 (1991) 881.
[21] G. Binash, P. Grünberg, F. Saurenbach, W. Zinn, Phys. Rev. B. 39 (1989) 4828.
[22] Proc. 15th Int. Colloquium on Magnetic Films and Surfaces, ICMFS '97, J. Physics D: Appl. Phys. 31 (1998)
[23] P. Bödeker, A. Abromeit, K. Bröhl, P. Sonntag, N. Metoki, H. Zabel, Phys. Rev. B 47 (1993) 2353.
[24] Th. Zeidler, F. Schreiber, H. Zabel, W. Donner, N. Metoki, Phys. Rev. B 53 (1996) 3256.